INSTITUT DE FRANCE
Académie des sciences

Comptes Rendus

Chimie

Elena-Florentina Grosu, Elena Seftel, Matthias Cuykx, Myrjam Mertens, Adrian Covaci, Pegie Cool and Gabriela Carja

Efficient degradation and mineralization of diclofenac in water on ZnMe (Me: Al; Co; Ga) layered double hydroxides and derived mixed oxides as novel photocatalysts

Volume 25, Special Issue S3 (2022), p. 51-67

Published online: 3 May 2022

https://doi.org/10.5802/crchim.167

Part of Special Issue: Active site engineering in nanostructured materials for energy, health and environment

Guest editors: Ioana Fechete (Université de Technologie de Troyes, France) and Doina Lutic (Al. I. Cuza University of Iasi, Romania)

Les Comptes Rendus. Chimie *sont membres du*
Centre Mersenne pour l'édition scientifique ouverte
www.centre-mersenne.org
e-ISSN : 1878-1543

Comptes Rendus
Chimie
2022, Vol. 25, Special Issue S3, p. 51-67
https://doi.org/10.5802/crchim.167

Active site engineering in nanostructured materials for energy, health and environment / *Ingénierie de sites actifs dans les matériaux nanostructurés pour l'énergie, la santé et l'environnement*

Efficient degradation and mineralization of diclofenac in water on ZnMe (Me: Al; Co; Ga) layered double hydroxides and derived mixed oxides as novel photocatalysts

Elena-Florentina Grosu [a, b], Elena Seftel [b, c], Matthias Cuykx [d], Myrjam Mertens [c], Adrian Covaci [d], Pegie Cool [b] and Gabriela Carja [*, a]

[a] Department of Chemical Engineering, Faculty of Chemical Engineering and Environmental Protection, Technical University "Gh. Asachi", Bd. Mangeron 71, Iasi 700554, Romania

[b] Laboratory of Adsorption and Catalysis, Department of Chemistry, University of Antwerpen (CDE), Universiteitsplein 1, 2610 Wilrijk, Antwerpen, Belgium

[c] VITO Flemish Institute for Technological Research, Boeretang 200, B-2400, Belgium

[d] Toxicological Centre, Department of Pharmaceutical Sciences, University of Antwerpen, Universiteitsplein 1, 2610 Wilrijk, Antwerpen, Belgium

E-mails: elena_grosu89@yahoo.com (E.-F. Grosu), elena.seftel@vito.be (E. Seftel), matthias.cuykx@uantwerpen.be (M. Cuykx), myrjam.mertens@vito.be (M. Mertens), adrian.covaci@uantwerpen.be (A. Covaci), pegie.cool@uantwerpen.be (P. Cool), carja@uaic.ro (G. Carja)

Abstract. The removal of diclofenac (DCF) from aqueous solutions was attempted using photocatalytic processes, involving a series of novel photocatalysts based on ZnMe (Me: Al; Co; Ga) layered double hydroxides (LDHs) and their derived mixed oxides. The catalysts were characterized using specific techniques. Under solar light, ZnCo and ZnGa catalysts degraded almost completely DCF from water, while the mineralization, expressed by total organic carbon removal, reached ~85%. The degradation mechanisms of DCF photolysis and photocatalytic degradation under solar and UV irradiation were investigated.

Résumé. L'élimination du diclofénac (DCF) de solutions aqueuses a été étudiée en utilisant des processus photocatalytiques, en utilisant une série de nouveaux photocatalyseurs basés sur d'hydroxydes doubles lamellaires ZnMe (Me : Al ; Co ; Ga) (LDH) et leurs oxydes mixtes dérivés. Les catalyseurs ont été caractérisés à l'aide de techniques spécifiques. Par irradiation en lumière solaire, les catalyseurs ZnCo et ZnGa ont dégradé presque complètement le DCF de l'eau, tandis que la minéralisation, exprimée par l'élimination totale du carbone organique, a atteint ~85%. Les mécanismes de dégradation

* Corresponding author.

de la photolyse du DCF et de la dégradation photocatalytique sous irradiation solaire et UV ont été étudiés.

Keywords. Diclofenac, Photocatalysts, Layered double hydroxides, Water pollution, Photosensitization.

Mots-clés. Diclofénac, Photocatalyseurs, Hydroxydes doubles lamellaires, Pollution de l'eau, Photosensibilisation.

Published online: 3 May 2022

1. Introduction

Environmental problems are more prevalent nowadays and one of the big concerns is water contamination by toxic compounds. Diclofenac (DCF) is a widely used non-steroidal anti-inflammatory drug (NSAID) that reached a worldwide consumption of ~1000 tons per year [1]. Only a fraction of the drug is absorbed and metabolized by humans or animals and the rest is excreted, either as metabolites or as unchanged parent compound. Currently, DCF residues are commonly detected in various aquatic environments [2,3]. The extended exposure of DCF, even at very low concentrations, has impacts on both human health and ecological safety [4]. Due to the high toxicity, DCF has been included on the European Union Water Framework Directive First watch list for emerging water pollutants so that, monitoring data need to be collected to understand its total impact [5]. Based on the recent global studies, the concentrations of DCF in water varied in the range of $ng{\cdot}L^{-1}$ to $\mu g{\cdot}L^{-1}$ [6,7] and the drug cannot be effectively eliminated by conventional sewage treatment plants [6]. Once it is released in water bodies, the degradation of DCF is insignificant. It has been reported that under sunlight exposure DCF is decomposed to metabolites sought to be more harmful to ecosystems and public health than DCF, thus the pollution and the toxicity of water increases [7,8]. The use of photocatalysts to remove DCF from water is regarded as a simple and cost-effective approach in the conditions that we will be able to exploit the properties of the catalysts to enhance their performances, but also to control the degradation pathways [9–11]. Recently, Sarasidis *et al.* reported that the DCF mineralization reached 69% on TiO_2 photocatalyst after 8 h of UV-light irradiation [12], while Salaeh *et al.* showed that TiO_2-zeolite/H_2O_2 catalytic system is able to mineralize 67% of DCF from aqueous solutions under solar light irradiation [13].

So far, studies on photocatalytic degradation of DCF have mainly focused on the removal kinetics and degradation/mineralization efficiency of the drug [12,14]. Though, to establish an effective solution for DCF degradation requires not only to design and optimize an efficient photocatalytic formulation, but also to look inside the photodegradation mechanism, with the identification of the photodegradation products, and the assessment of their possible effects. However, considering the low concentrations, the unknown chemical structure and fast transformation of intermediates, the accurate identification of degradation products is, certainly, a highly challenging task [8,9].

Our previous work demonstrated that 2-D matrices of layered double hydroxides (LDHs) and their derived oxides can be designed as successful photocatalysts for the removal of toxic pollutants [15, 16]. LDHs are a class of anionic clays with formula as $[M(II)_{1-x}M(III)_x \cdot (OH)_2]^{x+}(A^{n-})_{x/n} \cdot mH_2O$, and a controlled microstructure *via* regulating the nature and ratio of M(II), M(III) of brucite-like layers and A^{n-} intercalated anions [17]. Recently, there is increasing interest to prepare efficient photocatalysts based on Zn-rich LDHs with layers modified containing non-precious transition metals. Thus, we used Co^{2+} and Ga^{3+} to partially substitute Zn^{2+} and Al^{3+}, in order to increase the capability of Zn-based materials to harvest the light energy in photochemical processes [18].

In this study, we present ZnMe (Me: Al; Co; Ga) LDHs as novel and highly efficient photocatalysts for the degradation/mineralization of DCF in water by harvesting light energy. We compared the catalytic performances of the LDHs-like catalysts to that of the MMOs formed after the LDHs calcination at 750 °C. More importantly, the origin of the photocatalytic efficiency was explored by the investigation of the degradation mechanisms of DCF through the identification of the major intermediates by liquid chromatography quadrupole time-of-flight mass spec-

trometry (LC-MS). To the best of our knowledge, a synergic response of the catalyst and the type of light used for irradiation during DCF degradation in water is reported here for the first time.

2. Material and methods

2.1. *Materials*

$Zn(NO_3)_2{\cdot}6H_2O$, $Al(NO_3)_3{\cdot}9H_2O$, $Co(NO_3)_2{\cdot}6H_2O$, $Ga(NO_3)_3{\cdot}9H_2O$, NaOH, Na_2CO_3, and diclofenac were purchased from Sigma-Aldrich Chemical (>98% purity).

2.2. *Preparation of photocatalysts*

ZnMe (Me: Co; Ga; Al) LDHs were prepared via the co-precipitation method [17–19] at 65 °C and a constant pH of 9 [15,16]. ZnAl LDHs, molar ratio of Zn^{2+}/Al^{3+} = 2/1 and 3/1, were obtained by the slow addition of an aqueous solution of $Zn(NO_3)_2{\cdot}6H_2O$ and $Al(NO_3)_3{\cdot}9H_2O$ to an aqueous solution of $NaOH/Na_2CO_3$ and denoted as $ZnAl_2$ and $ZnAl_3$, respectively. Next, the ZnCo catalyst was obtained by the partial substitution of Zn^{2+} with Co^{2+}, when $Co(NO_3)_2{\cdot}6H_2O$ was added as a source of Co^{2+} in the starting aqueous solutions, to reach a molar ratio of Zn^{2+}/Co^2 = 1/1 and $(Zn + Co)^{2+}/Al^{3+}$ = 2/1. Furthermore, the ZnGa photocatalyst (Zn^{2+}/Ga^{3+} = 3/1) was obtained by replacing Al^{3+} with Ga^{3+} in the clay layers, using $Ga(NO_3)_3{\cdot}9H_2O$ in the staring solution. The resulting precipitates were aged for 24 h at 45 °C, washed and dried at 90 °C. To obtain the mixed oxides the "as synthesized" LDHs were calcined at 750 °C for 10 h. This high calcination temperature was used in order to obtain highly crystallized mixed oxides. The evolved mixed oxides were denoted as following: $ZnAl_2$-750, $ZnAl_3$-750, ZnCo-750 and ZnGa-750.

2.3. *Characterization of photocatalysts*

Structural characteristics, composition, crystallinity, purity information and the thermal behavior of the catalysts were investigated by X-ray Diffraction (XRD), Energy Dispersive Spectroscopy (EDX), UV–vis Diffuse Reflectance spectroscopy (UV–Vis DR), Infrared Spectrometry (FTIR) and thermogravimetric TG/DTG analysis. The chemical composition was examined using an energy-dispersive X-ray spectrometer (EDX) device attached to the microscope. X-ray diffractions were performed on a PANalytical X'Pert PROMPD diffractometer equipped with a filtered Cu Kα radiation, λ = 0.15406 nm; measurements were done in the 2θ mode using a bracket sample holder with a scanning speed of 0.04°/4 s in continuous mode. UV–Vis DR absorption spectra were recorded on a Nicolet Evolution 500 UV–vis spectrometer, equipped with a DR accessory and considering KBr as white reference. TEM results were obtained on a Model H-7650, Hitachi operating at 100 kV. The samples were mounted on a conducting carbon with Cu grid mesh (150 mesh per inch) and tungsten filament was used in the electron gun. Diffuse Reflectance Infrared Fourier Transform spectra (DRIFT) were measured on a Nicolet 6700 FT-IR spectrometer, equipped with a mid-IR source (400–4000 cm^{-1}), a KBr-beam splitter, a He/Ne laser with a Michelson interferometer. About 200 scans were taken with a 4 cm^{-1} resolution. TG/DTG measurements were performed on a Mettler Toledo TGA/SDTA851 thermobalance; samples were heated from 30 to 850 °C with a heating rate of 10 °C/min, under O_2 flow.

2.4. *Photocatalytic activity evaluation*

The photocatalytic activity of the studied materials was tested for DCF photodegradation in aqueous medium. In a typical experiment, the catalyst (1 g/L) was dispersed in a DCF solution with a concentration of 0.025 g DCF/L and stirred in the dark to reach adsorption equilibrium, and then the reaction was started. For this, the catalyst/DCF aqueous medium was irradiated with an Unnasol US 800 solar simulator, 250 W, equipped with visible block-filters, such that both solar and UV-light energy were used for irradiation. The reactions were carried out in 200 mL reactor and the reaction temperature was maintained at 25 °C by circulating water. At selected time intervals, 2 mL of the suspension was withdrawn and centrifuged to remove the catalyst.

2.4.1. *Evaluation of %DCF removal by UV–Vis absorption spectroscopy*

The DCF concentration in the supernatant solutions was monitored by a UV–Vis spectrophotometer at maximal absorption band of 276 nm for the UV driven tests and at 236 nm for the solar driven tests, due to the shift of the absorption band, when

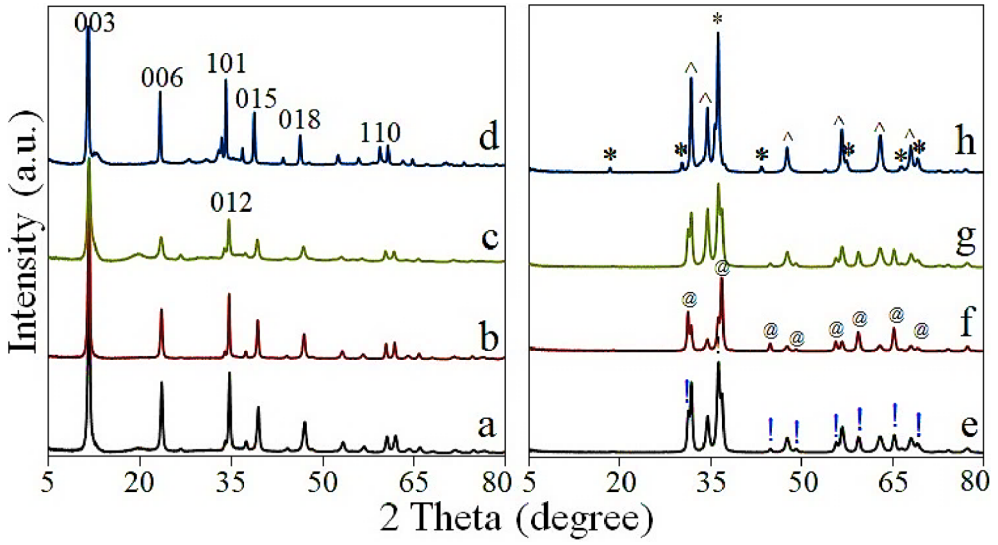

Figure 1. X-ray diffraction patterns of: (a) $ZnAl_2$, (b) ZnCo, (c) $ZnAl_3$, (d) ZnGa, (e) $ZnAl_2$-750, (f) ZnCo-750, (g) $ZnAl_3$-750, (h) ZnGa-750; (!) $ZnAl_2O_4$, (@) $CoAl_2O_4$, (*) $ZnGa_2O_4$ and (^) ZnO.

different intermediates are produced during the photodegradation process.

2.4.2. *Evaluation of %DCF mineralization by TOC analysis*

Total Organic Carbon (TOC) measurements were done with Shimadzu TOC-Vcph. We obtained the TOC values by measuring the TC (total carbon) and the IC (inorganic carbon) and subtracting the IC concentration from the TC concentration. The TC and IC analysis were performed at the beginning and at the end of the test. In this way, the TOC initial and TOC final (after 4 h of irradiation) were determined. The mineralization yield was calculated as the difference between TOC initial and TOC final divided by TOC initial.

2.4.3. *Evaluation of DCF removal process by LC-MS analysis*

Liquid chromatography quadrupole time-of-flight mass spectrometry (LC-MS) was employed for the identification of the photodegradation products resulting from DCF decomposition. We used the method and parameters described by Alvarez-Martin *et al.* [20], and they are presented in Section S1.

3. Results and discussions

3.1. *Characterization of the photocatalysts*

The EDX results (see Supplementary Figure S2) show that the catalysts have a high Zn content equal of 50 ± 5 wt%. Meanwhile, besides Zn, only Co, Al, Ga and O are detected. The XRD patterns of the studied photocatalysts are shown in Figure 1. As seen, the "as-synthesized" LDHs show (see Figure 1a–d) a high crystallization degree due to the strong diffraction peaks that define the typical characteristics of the LDHs-like phase (ICDD file no. 22-700) [17] with a series of sharp and symmetric basal reflections of the (003), (006), (101) planes at 11.7°, 23.6°, 34.1° and broad, less intense, reflections for the nonbasal (012), (015), (018), (110) planes around 34.7°, 39.2°, 46.9°, 60.6°. The interlayer distance was calculated using the (003) basal reflection from 11.7° and the value is ~0.76 nm for all the synthesized LDHs. This indicates the presence of CO_3^{2-} as interlayers anion in the LDH-type catalysts [17].

Table 1 shows the molar ratio between the bivalent and trivalent cations of the LDHs layers obtained from EDX and the "*a*" and "*c*" parameters that define the LDH structure [17,21]. The presence of Ga^{3+} into the LDHs layers is revealed by the increase of the "*a*" parameter, due to the larger ionic radius of Ga^{3+} than that of Al^{3+} (0.62 vs 0.53 Å). On the other hand, Zn^{2+}

and Co^{2+} possess similar ionic radius (0.74 vs 0.745 Å) hence the "*a*" parameter of ZnCo and $ZnAl_2$ has similar values. The cobalt content was clearly confirmed by EDX (Figure S2) and is consistent with the content of the $Co(NO_3)_2{\cdot}6H_2O$ from the starting solution. The thermal treatment at 750 °C gives rise to the destruction of the LDHs-like network and the formation of the mixtures of mixed oxides (MMOs) where the characteristic diffractions (see Figure 1e–h) of (!) $ZnAl_2O_4$, (@) $CoAl_2O_4$, (*) $ZnGa_2O_4$ and (^) ZnO are clearly assessed. DRIFT results (see Figure S3) show that all the LDHs-like catalysts have CO_3^{2-} as anions in the interlayers with the intense vibration band at 1360 cm^{-1} and less intense vibration band at 1510 cm^{-1}, corresponding to the CO_3^{2-} symmetric and antisymmetric bending vibrations, respectively [16]. The broad absorption band, which may be associated to the O–H stretching of the hydroxyl groups from the brucite-like layers and physisorbed interlamellar water [17] is clearly observed within (3000–3500) cm^{-1}. The small broad shoulder centered around 1640 cm^{-1} is assigned to H–O–H bending vibration of interlayer water molecules. The corresponding vibrations of the Me–O and O–Me–O (Me: Zn, Co, Al, Ga) were observed in the low wavenumber region inside the range (800–400) cm^{-1} [17,22]. Therefore, the results of XRD, DRIFT and EDX analyses point out that ZnAl, ZnCo and ZnGa catalysts are highly crystallized LDH-like structures with CO_3^{2-} as main anion of the interlayers. The morphological characteristics of the LDHs-like catalysts can be seen in the TEM images in Figure 2a,b. It shows the presence of irregularly aggregated and interconnected nanoplates with an average size of 90 nm. These features are typical for the LDHs materials [16,17]. After calcination at 750 °C it can be seen (Figure 2c,d) that for the derived MMOs the particles become smaller, with a size of around 50 nm.

To get more insight into the transformation of the LDHs to MMOs we examined the results of the TG-DTG analysis given in Supplementary Figure S4. Firstly, the mass loss is described by the three stages. The first mass loss, from room temperature to approximately 230 °C, is mainly assigned to the removal of the interlayer and weakly adsorbed water. The second stage of mass loss, which occurs in the temperature range 200–340 °C, is showing the dehydroxylation of the LDHs lattice, while the third loss is revealing that the MMOs crystallized in the temperature range 430–800 °C. This revealed that the LDH-like catalysts progressively lost the physisorbed water, then the interlamellar water and further the water from the dehydroxylation of the layers, along with the charge compensating anions. This led to the collapse of the layered structure of LDHs and the formation of the Zn-rich solid solutions of MMOs-like catalysts. Secondly, the DTG profiles indicate three weight losses with features that revealed that the temperature ranges for the removal of interlayer water and dehydroxylation of the lattice are shifted to lower temperature for ZnCo and ZnGa in comparison to $ZnAl_2$ and $ZnAl_3$, respectively.

Table 1. Chemical composition and the lattice parameters of the studied photocatalysts

LDHs	M^{2+}/M^{3*}	Lattice parameters (Å)**	
		a	*c*
$ZnAl_2$	1.75	3.056	22.5
ZnCo	1.8	3.064	22.5
$ZnAl_3$	2.7	3.068	22.65
ZnGa	3.1	3.112	22.86

*The molar ratio between the bivalent and trivalent cations in the LDHs layers, from EDX.

**a = 2d110 and c = 3d003 are the unit lattice parameters.

Further, the optical responses of the catalysts is studied by UV–Vis DR (see Figure 3). The LDHs-like catalysts have a lower absorption in the UV region compared to that of the derived MMOs that show a distinct wide absorption in the Vis region, well above 420 nm that agrees to previous results [23,24]. For ZnCo the band centered at about 520 nm is similar to that observed in the UV–visible spectrum of octahedrally coordinated Co^{2+}. According to Ulibarri *et al.* this band is assigned to the $^4T_{1g}(F) \rightarrow {}^4T_{1g}(P)$ transition of octahedrally coordinated Co^{2+} from the LDH layers [25]. For the mixed oxides obtained after the calcination, the intense band around 360 nm might be attributed to the Zn–O charge transfer band in the mixture of ZnO and $ZnAl_2O_4$ or $ZnGa_2O_4$ [22]. Furthermore, Figure 3b shows that $ZnAl_2$-750 and $ZnAl_3$-750 absorbed only in UV region though ZnCo-750 and ZnGa-750 absorbed in the visible region well above 500 nm with the absorption edge that shifts to longer wavelengths.

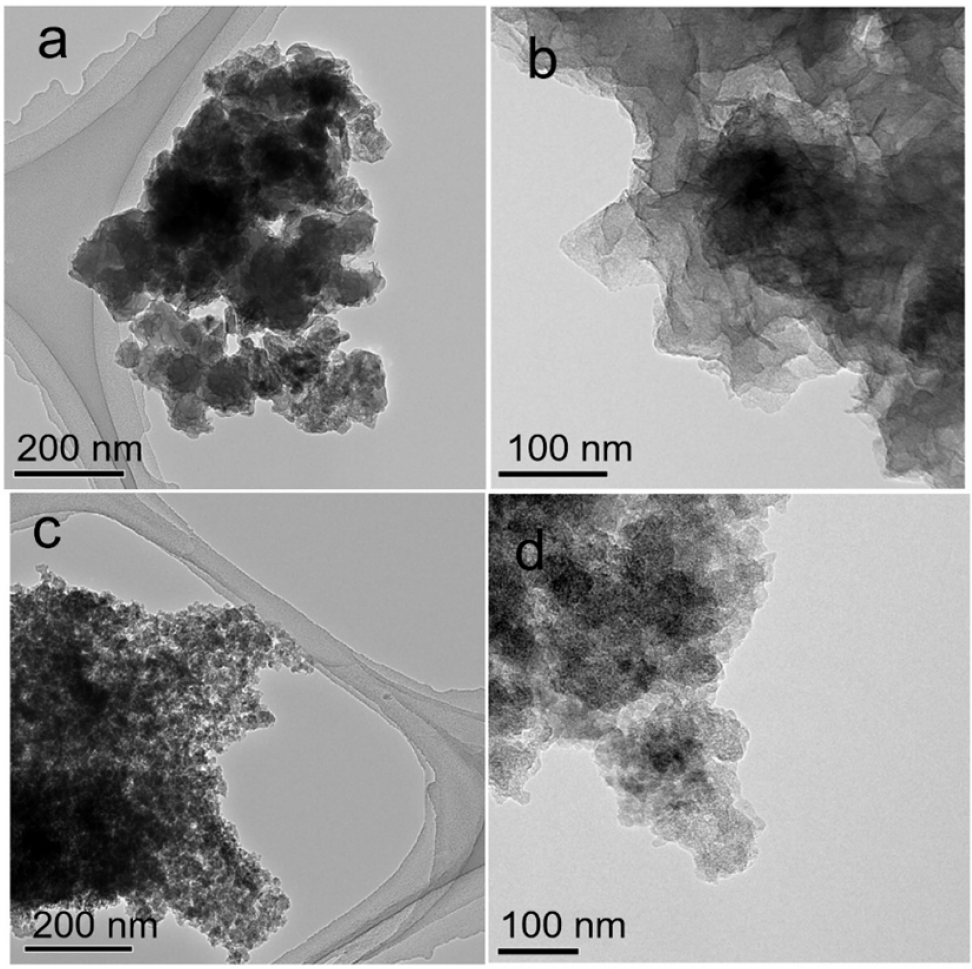

Figure 2. Typical TEM images of ZnCo (a,b); ZnCo-750 (c,d).

3.2. *Photocatalytic degradation/mineralization of DCF in water*

Under irradiation by simulated solar light, the efficiency of the degradation/mineralization of DCF in water is shown in Figure 4A. Results show that all catalysts have the capability to degrade more than 90% of DCF.

Among these, ZnCo and ZnGa show the best activity reaching 96% and 95% DCF degradation. The mineralization yields, investigated by TOC measurements, were 77% and 67% for $ZnAl_3$ and $ZnAl_2$, respectively, indicating that the DCF mineralization increased with the increase of Zn content. Further, DCF mineralization increases with the introduction of Co and Ga in the LDHs layers up to 84% and 86%, respectively, with ZnGa and ZnGa750 highly active in both s synthesized and the calcined form, respectively. This clearly shows that the LDHs composition is dominantly responsible to establish a performant photocatalyst for the removal of DCF from water.

Table 2 shows the results of the best performing catalysts in comparison to that obtained on other catalytic systems reported in the last years [11,12, 26–34]. It is noticed that the catalysts studied in this work are highly performant for DCF removal from water as demonstrated by the high photodegradation/mineralization yields obtained under solar light irradiation.

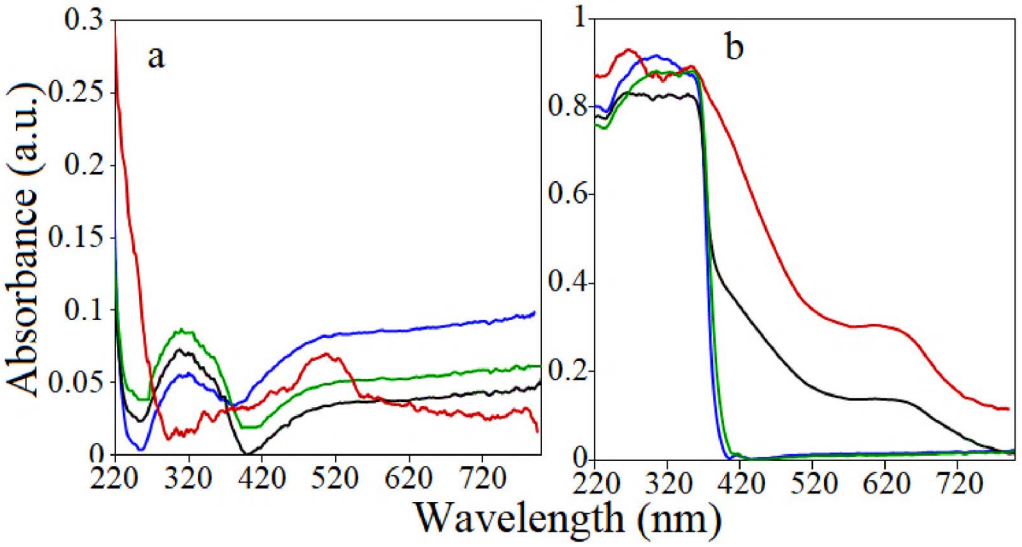

Figure 3. UV–Vis DR spectra: (a) ( ) $ZnAl_2$, ( ) ZnCo, ( ) $ZnAl_3$, ( ) ZnGa; (b) ( ) $ZnAl_2$-750, ( ) ZnCo-750, ( ) ZnGa-750, ( ) $ZnAl_3$-750.

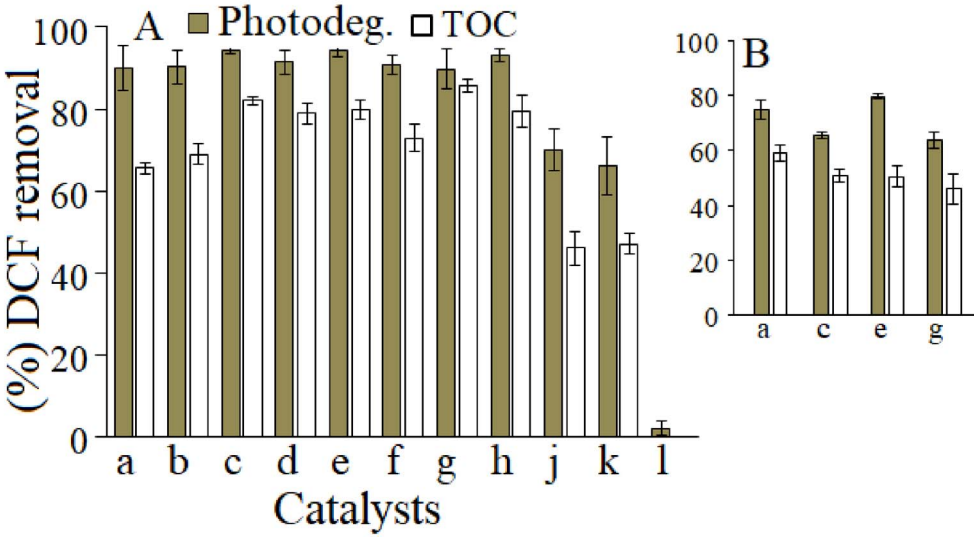

Figure 4. % DCF removal from aqueous solution after irradiation for 4 h by (A) solar light; (B) UV light. (a) $ZnAl_2$, (b) $ZnAl_2$-750, (c) ZnCo, (d) ZnCo-750, (e) ZnAl(3/1), (f) $ZnAl_3$-750, (g) ZnGa, (h) ZnGa-750, (k) P25, (j) g-C3N4, (l) blank.

Furthermore, the modification of the catalyst structure by calcination reveals that the capability of the MMOs to mineralize DCF is lower in comparison to that of the LDHs-like catalysts. The chemical composition of the LDHs and their derived MMOs is slightly similar. Thus, we can assume that the catalyst structure is a key factor for establishing the catalyst ability to mineralize DCF under irradiation by solar light. Catalysts as P25 and g-C_3H_4 were also tested in this study, but their performance in DCF photocatalytic degradation is inferior to that of LDHs based catalysts. It is also important to note that in the ab-

Table 2. Comparison of some recent results of the DCF photocatalytic degradation/mineralization in water

Photocatalyst	Dose, g/L	Irradiation source	DCF initial, mg/L	% DCF removal, Phot[a] or TOC[b]	Ref.
HApT (TiO_2 based catalyst)	4 g	XX-15 BLB UV lamp, 1.80 mW/cm^2	5	98%/24 h-Phot	[26]
TiO_2	Not given	0.7 kW UV lamp, λ = 254 nm, 2 mW·cm^{-2}	50	80%/3 h-Phot	[27]
CQDs/BiOCOOH	0.6	350 W Xe-lamp, 1.15 mW·cm^{-2}, $\lambda > 420$	4	98%/1 h-Phot	[28]
CQDs-C3N4	0.2	300 W Xe lamp, 150 ± 5 mW/cm, $\lambda > 400$ nm	10	100%/1 h-Phot	[29]
N, S, C-ZnO + $K_2S_2O_8$ and H_2O_2	0.44	UV mercury vapor lamp	20	98%/2 h-Phot	[30]
TiO_2–SnO_2	0.8	UV lamp	20	90%/5 h-TOC	[31]
Fe_3O_4/Ti_xO_x-activated carbon fiber	1.5	UV photoreactor	4.7	96%/2 h-Phot	[35]
Mg–SiTi	0.7	125 W Hg lamp, $\lambda < 420$ nm	20	50%/1 h-Photo	[32]
TiO_2	0.5	24 W UV lamp	2	70%/4 h-TOC	[12]
Zn/Al–La mixed oxides	1	20 W black light fluorescent, λ = 365–465 nm	50	88%/3 h-Phot	[33]
ZnO–WO_3	0.8	Visible light, 400 W	20	76%/4 h-TOC	[11]
ZnGa	1	250 W solar lamp	25	86%/4 h-TOC	This study
ZnCo	1	250 W solar lamp	25	84%/4 h-TOC	This study

[a]Phot = photodegradation; [b]TOC = mineralization.

sence of the catalyst, the DCF degradation in water is less than 2%. Supplementary Figure S5 shows the UV–Vis spectra profiles for the photodegradation of DCF in water under solar light for the studied catalysts. The profiles have particular features suggesting that each catalyst promoted specific DCF degradation pathways. Next, the % removal of DCF from water in the presence of ZnLDH, under irradiation by UV-light is given in Figure 4b. As shown, under simulated UV light, the catalysts' efficiency was lower, with a maximum of TOC value of 61% for $ZnAl_2$, while ZnCo and ZnGa degraded 67% and 65%, while the mineralization yield of DCF was 54%. This reveals that besides the catalyst properties, the type of light energy used for irradiation (solar or UV) might further impact the intermediate products of the DCF removal pathways.

3.3. *Mechanism of DCF photocatalytic degradation in water*

It is generally accepted that a photodegradation process occurs due to the adsorption of the pollutant molecules on the surface of the catalyst, followed by the formation of the oxidative species induced by the migration of light-generated electron–hole pairs. The elimination of the organic compounds by photocatalysis is the result of the oxidation properties of photocatalytically generated reactive species (RSs), such as h^+, •OH and O_2•. These species interact with the adsorbed pollutant molecules, transforming them into products [36,37]. Nevertheless, the contribution of each RS is still unclear and dependent on the type of the pollutant [36,37]. In the case of DCF photodegradation, the obtained results suggest that two processes might take place, having a synergetic

effect over the removal process: photosensitization (see (1)–(6)) and photooxidation (see (7)–(11)). These events are presented in Figure 5 and they are initiated by photosensitization, that means the light interaction with DCF, or by the interaction of DCF with the solid catalyst, hence, photooxidation. Hence, the photosensitization process of DCF starts under solar irradiation, when the excited ($DCF^{\bullet}$) transfers its electrons onto the conduction band of the catalysts, promoting the formation of the oxidized species (1)–(6).

$$DCF + LDHs \rightarrow DCF/LDHs \quad (1)$$

$$DCF/LDHs + h\nu \rightarrow DCF^{\bullet}/LDHs \quad (2)$$

$$DCF^{\bullet}/LDHs \rightarrow DCF^{\bullet+} + LDHs(e^{-}_{CB}) \quad (3)$$

$$LDHs(e^{-}_{CB}) + O_2 \rightarrow O_2^{\bullet-} + LDHs \quad (4)$$

$$DCF^{\bullet+} \rightarrow \text{products} \quad (5)$$

$$DCF^{\bullet+} + O_2^{\bullet-} \rightarrow \text{products} \quad (6)$$

$$DCF/LDHs + h\nu \rightarrow DCF/LDHs \times (e^{-}_{CB} + h^{+}_{VB}) \quad (7)$$

$$DCF/LDHs(h^{+}_{VB}) + H_2O \rightarrow DCF/LDHs + OH^{\bullet} + H^{+} \quad (8)$$

$$OH^{\bullet} + DCF \rightarrow \text{products} \quad (9)$$

$$DCF/LDHs(e^{-}_{CB}) + O_2 \rightarrow DCF/LDHs + O_2^{\bullet-} \quad (10)$$

$$O_2^{\bullet-} + DCF \rightarrow \text{products} \quad (11)$$

When the excitation source interacts directly with the LDH composite, a transfer of electrons from the valence band to the conduction band is initiated, with the generation of electron–hole pairs. These species will further lead to the formation of strongly superoxide and oxidizing hydroxyl radicals which will participate in the DCF removal process (7)–(11). In brief, the generation of the high reactive •OH and $O_2^{\bullet-}$ species would be dominantly responsible for DCF photodegradation from water in the presence of the catalyst. Based on the above, we further selected ZnCo as one of the best performant catalysts to study the mechanistic degradation pathways and to identify the degradation products. The identification of degradation products was challenging and was performed by HRMS analysis. These results were correlated with the UV–Vis degradation profiles as seen in Figure S5. Retention times and the molecular formula of the degradation intermediates with the corresponding the m/z values are given in Supplementary Table S6.

3.4. *DCF photodegradation pathways*

3.4.1. *DCF photolysis degradation pathway under solar light irradiation*

Prior to the photocatalytic tests, a blank test was carried out, when the DCF solution was irradiated by solar light, in absence of any solid catalyst. The results obtained by UV–Vis analysis (see Figure 6a) show that only 2% of DCF was degraded after 4 h of solar irradiation. Using LC-MS analyses, 21 degradation intermediates are identified, which are shown in Figure 6b and further described as S1 group in Supplementary Information, Table S6. At the end of the photocatalytic test (4 h solar irradiation), the LC-MS analysis revealed the only 11 products were still present in water, belonging to carbazoles and quinine imines classes. This finding agrees to the results reported by Alharbi *et al.* showing that, under solar light, DCF is decomposed to highly toxic organic compounds which are stable in water [38]. These intermediates and the degradation pathway are proposed in Figure 7. The first path involves the ring hydroxylation and the ring closure [13] which can start with DCF or P16 (m/z 252), its decarboxylated intermediate. Considering the first route, the 2-[2-(2′,6′-dichloroanilino)-5-hydroxyphenyl]acetic acid (P10, m/z 312) is oxidized to 2-(1-(5-oxo-cyclohexa-1,3-dienyl-2-(2′,6′-dichloro-phenylimino)acetic acid (P12, m/z 310), which by losing the carboxylate ion leads to compound P13 (m/z 282). This structure undergoes further oxidation to compound P14 (m/z 280), which is a stable quinine imine intermediate [39]. The second path implies the elimination of a chlorine atom from DCF or product P16, followed by the ring closure, giving rise to the formation of carbazole products [40] identified in Figure 7 as P17 (m/z 215), P18 (m/z 211), P19 (m/z 227). Furthermore, we identified the formation of products belonging to the quinine imine class [41,42] denoted as P12, P13, P14 (m/z 310, 282, 280), the dechlorination products P1 (m/z 261), P2 (m/z 238) and hydroxylation/oxidation compounds as P16, P20 (m/z 268), P21 (m/z 266).

3.4.2. *DCF photocatalytic degradation pathway on ZnCo catalyst under solar light irradiation*

The DCF degradation pathways with ZnCo catalyst and under solar light irradiation was further investigated. The results of UV–Vis correlated with the

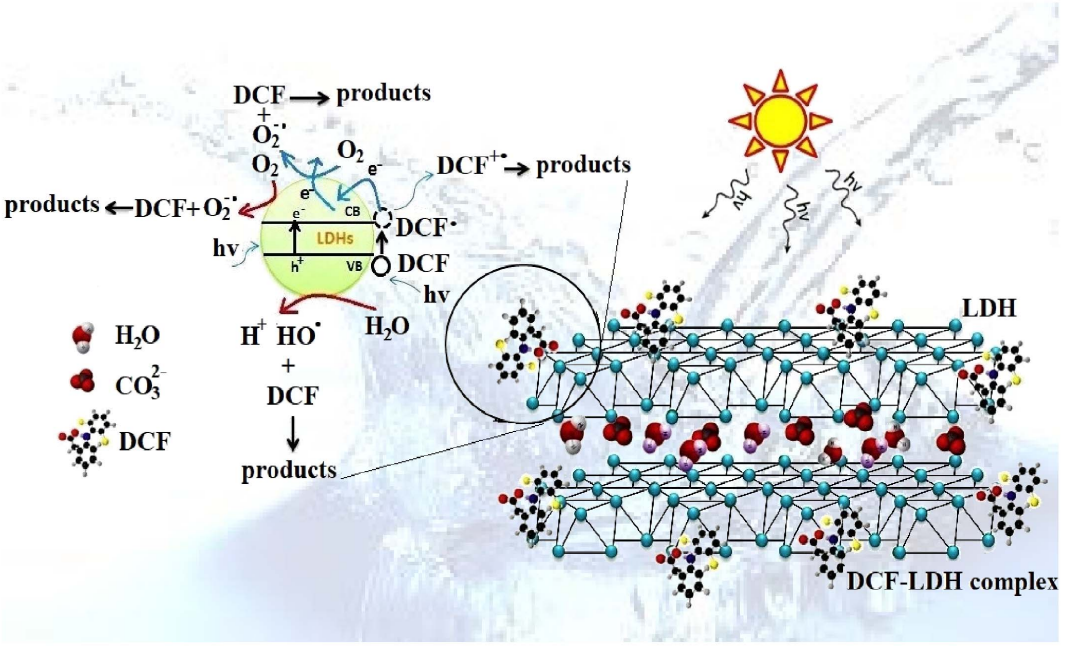

Figure 5. The proposed mechanism for the photocatalytic mineralization of DCF under solar light by combining the photosensitization and photooxidation processes.

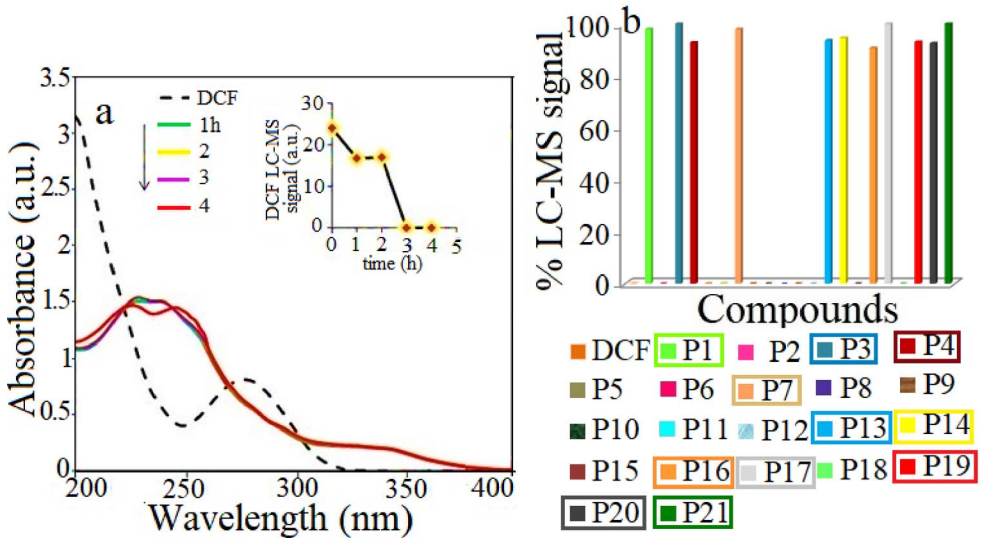

Figure 6. (a) UV–Vis profiles of DCF photolysis and (b) the corresponding % LC-MS products signal obtained under irradiation by solar light in the absence of catalysts (blank test); the products identified at the end of the catalytic test are marked within rectangles.

LC-MS observations are shown in Figures 8a and b, respectively.

These results show that DCF degrades in the presence of the catalyst and solar light irradiation into thirty intermediates, but at the end of the reaction,

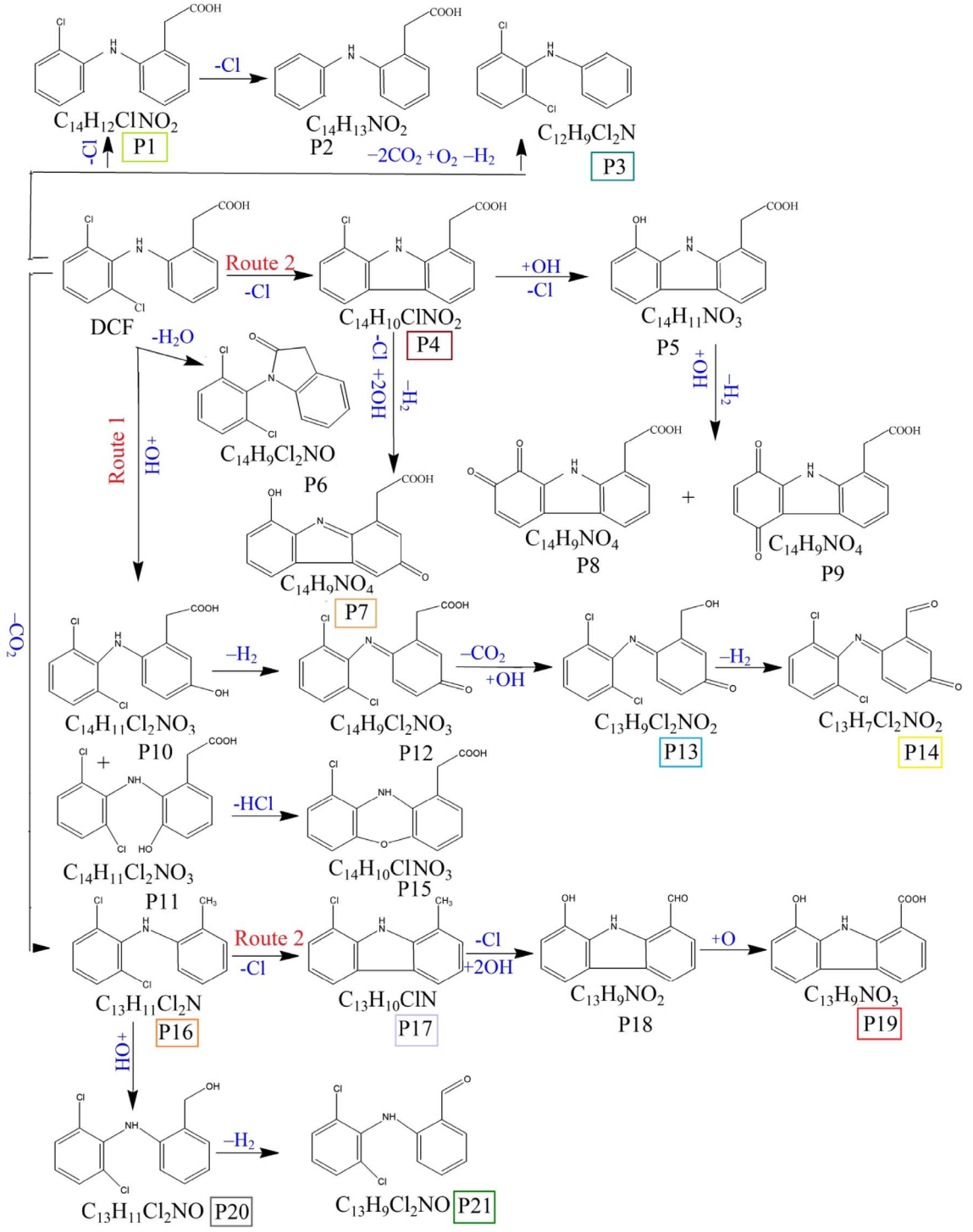

Figure 7. Proposed pathways for the mechanism of DCF photolysis under simulated solar light in the absence of catalyst (blank test).

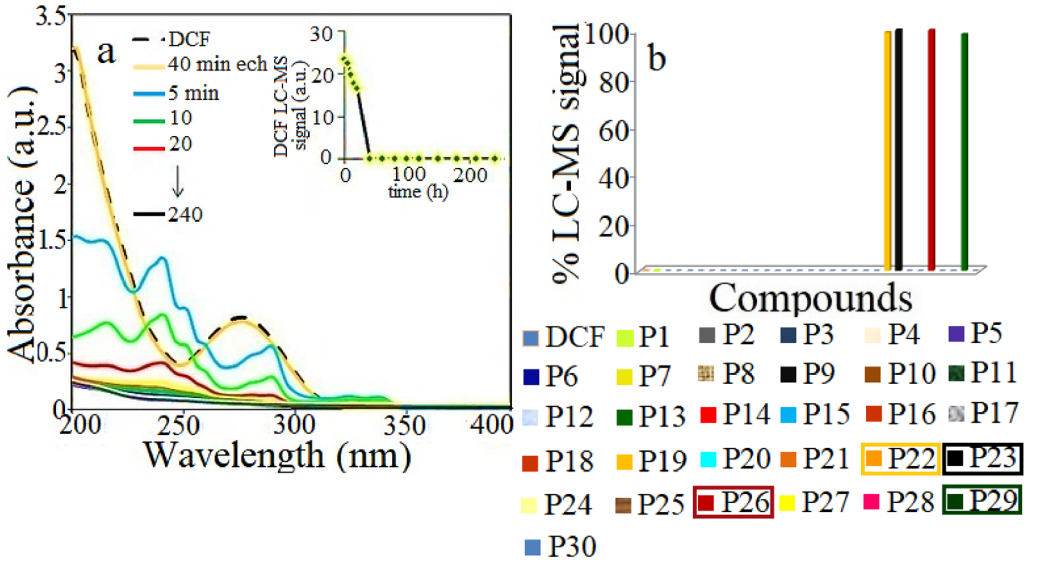

Figure 8. (a) UV–Vis spectra profiles of DCF photodegradation on ZnCo catalyst under simulated solar irradiation and (b) the corresponding % LC-MS signal of products; catalyst dose 1 g/L; DCF concentration of 0.025 g/L; the products identified at the end of the catalytic test are marked within rectangles.

only four major products are identified by LC-MS as m/z 179, m/z 140, m/z 168, m/z 118, highlighted in Figure 8b with rectangles. The identified intermediates are described in Supplementary Table S6 as group S3. Taking into account these intermediates, the hypothetical degradation pathways of DCF in water, in the presence of the ZnCo catalyst and solar light irradiation is proposed in Figure 9. Firstly, it assumes the ring closure of DCF and the formation of the decarboxylated intermediate P9 (m/z 252). It suggests further the generation of carbazole compounds which are described as system S2 in Table S6 and include: P5, (m/z 259), P6, (m/z 241), P7, (m/z 238), P8, (m/z 225) and P10, (m/z 215), respectively. Next steps show the NH-cleavage [38,40] as well as the ring opening when (1Z)-1-propene-1,2,3-tricarboxylic acid (P27, m/z 174), malic acid (P28, m/z 134), succinic acid (P29, m/z 118) and hexanoic acid (P30, m/z 116) are identified. Finally, these small molecules could be completely mineralized to CO_2 and H_2O.

3.4.3. *DCF photocatalytic degradation pathway on ZnCo catalyst under UV light*

Under UV light and in the presence of the catalyst, the DCF photodegradation profile shows similar UV–Vis spectra as the standard DCF solution (see Figure 10a). This indicates that, besides the derived metabolites, DCF is also present in the aqueous solution during the irradiation and at the end of the photocatalytic test. This is further confirmed by LC-MS results revealing the formation of a high number of intermediates, as well as the presence of DCF, as described in Figure 10b.

The proposed pathways are depicted in Figure 11 and include hydroxylation, dehydrogenation, decarboxylation, dechlorination and ring closure and further a N–H cleavage step. Therefore, under UV-light irradiation and in the presence of the catalyst, the formation of carbazoles e.g.: P1 (m/z 259), P2 (m/z 241), P4 (m/z 225) P5 (m/z 278), P8 (m/z 215) and quinine imine e.g.: P14 (m/z 310), P15 (m/z 282), P17 (m/z 280) structures were detected as intermediates and labeled in the Supplementary Table S6 as group S2. Furthermore, the N–H cleavage leads to the formation of smaller molecules e.g.: N-(2,6-dichlorophenyl) formamide (P18, m/z 190), 2,6-dichlorohydroquinone (P19, m/z 179), chlorobenzene (P25, m/z 112). The identified products at the end of the photocatalytic test are highlighted in Figure 9b within rectangles. These products are present in the aqueous media together with DCF that is only partially mineralized.

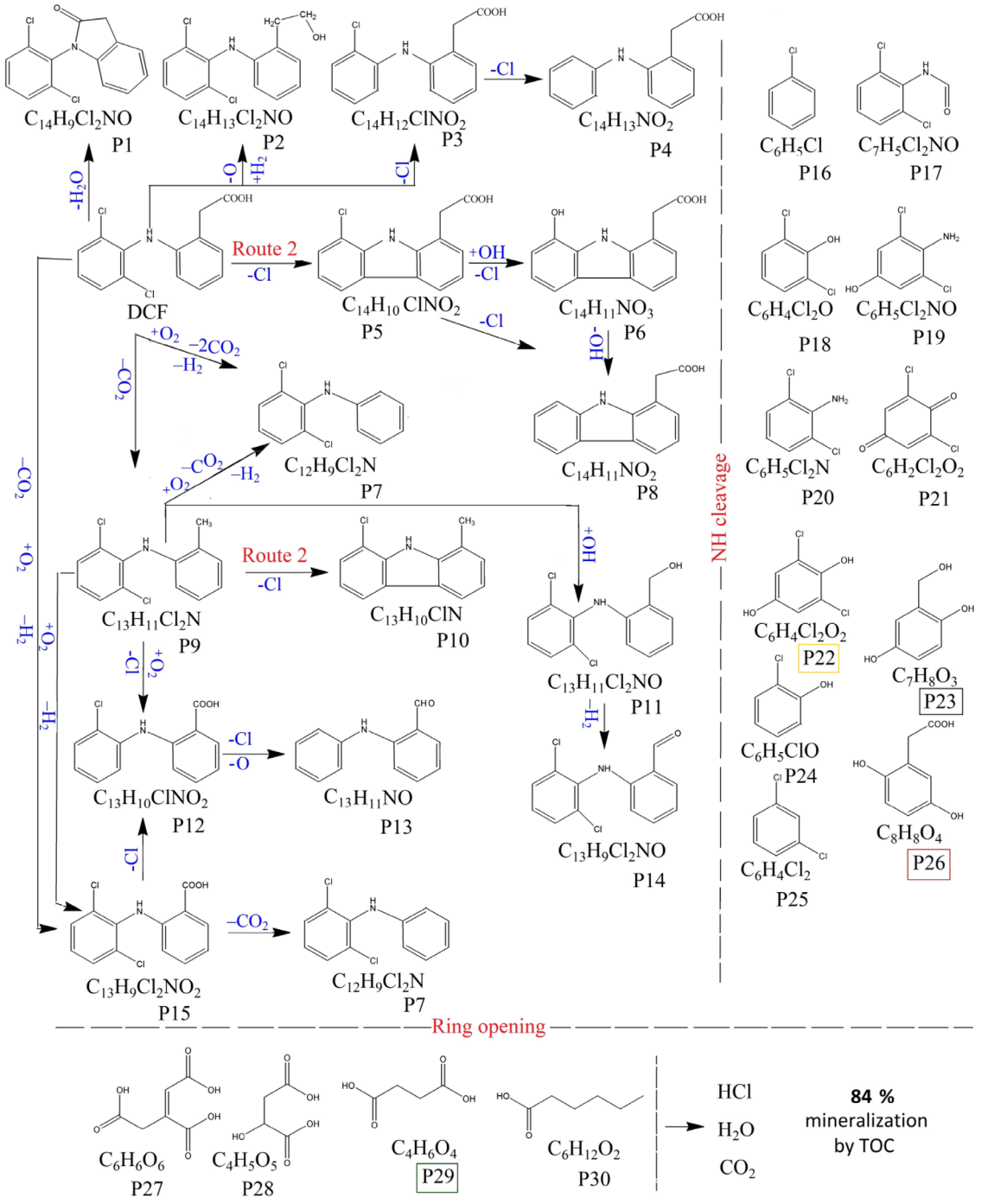

Figure 9. Proposed pathways for the mechanism of DCF photodegradation on ZnCo catalyst under simulated solar light irradiation.

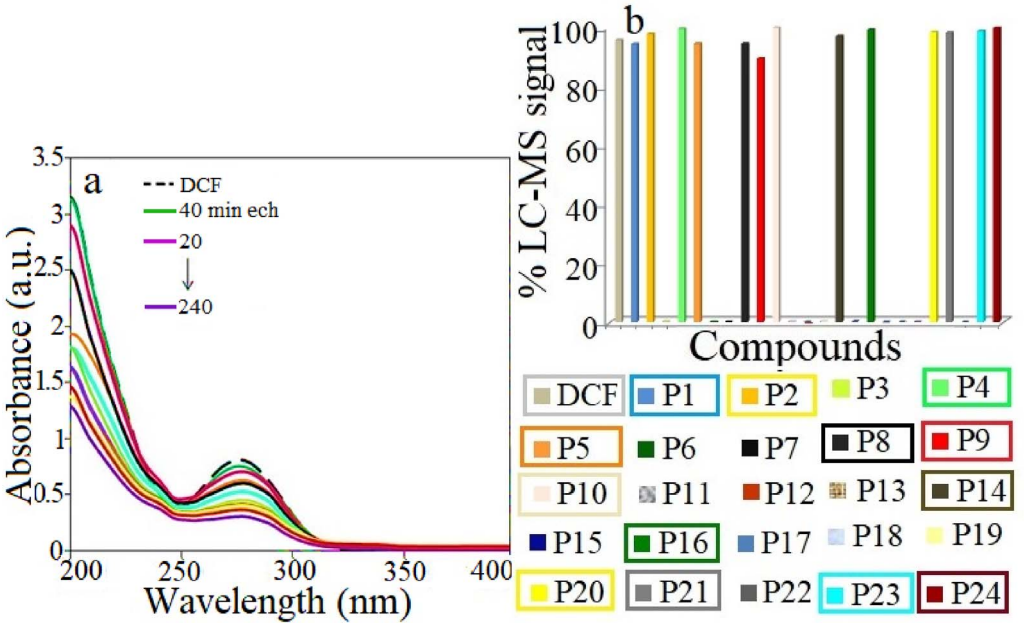

Figure 10. (a) UV–Vis spectra profiles of DCF photodegradation on ZnCo catalyst under simulated solar irradiation and (b) the corresponding % LC-MS signal of products; catalyst dose 1 g/L; DCF concentration of 0.025 g/L; the products identified at the end of the catalytic test are marked within rectangles.

These results demonstrate that LDHs-like catalysts with tailored chemical characteristics can create synergistic effects in the presence of solar light irradiation and can act as highly efficient photocatalysts for the complete removal of emerging water pollutants, like DFC as well as their metabolites. Furthermore, the high efficiency of these photocatalysts is also highlighted by the low solid/liquid ratio required, e.g. of only 1 g/L. This can lead to drug mineralization within mg (milligram) range (0.025 g DCF/L) suggesting that a very low amount of the catalyst will be capable to decontaminate large amount of wastewaters contaminated with DCF. Hence, is offering a viable solution for large scale decontamination of DCF from aqueous media. In this regard, it should be noted that the reported concentrations of the specific pollutants in wastewater effluents and freshwater rivers or canals are in the μg (microgram) or even ng (nanogram) range [43].

3.5. *Catalyst stability*

To evaluate the catalyst stability, ZnCo composite was chosen as reference and used for 4 consecutive tests, in the same conditions. Between each test, the catalyst was recovered, washed and reused. The data in Figure 12 shows that the catalysts were proven to show a high catalytic activity.

4. Conclusions

This study provides new insights into the solar-light-driven photocatalysis with LDH-type structure and ZnMe (Me: Al; Co; Ga) composition. These composites are showing superior or comparable activity for degrading DCF from water in comparison with the state of the art reported so far. The LDHs photocatalysts were synthesized by simple and cost-effective route and their structural features were investigated using the combination of SEM/EDX, XRD, FTIR, TG-DTG, TEM and UV–Vis DR techniques. Further, by exposing the synthesized LDHs to controlled thermal treatment, the corresponding mixed oxides (MMOs) were obtained. When tested for photodegradation of DFC in water, it was observed that the photocatalyst structure plays a key role in the mineralization process of DFC under solar light irradiation. The insertion of Co^{2+} within the structure and the presence of hydroxylated layers in the LDH structure, favored

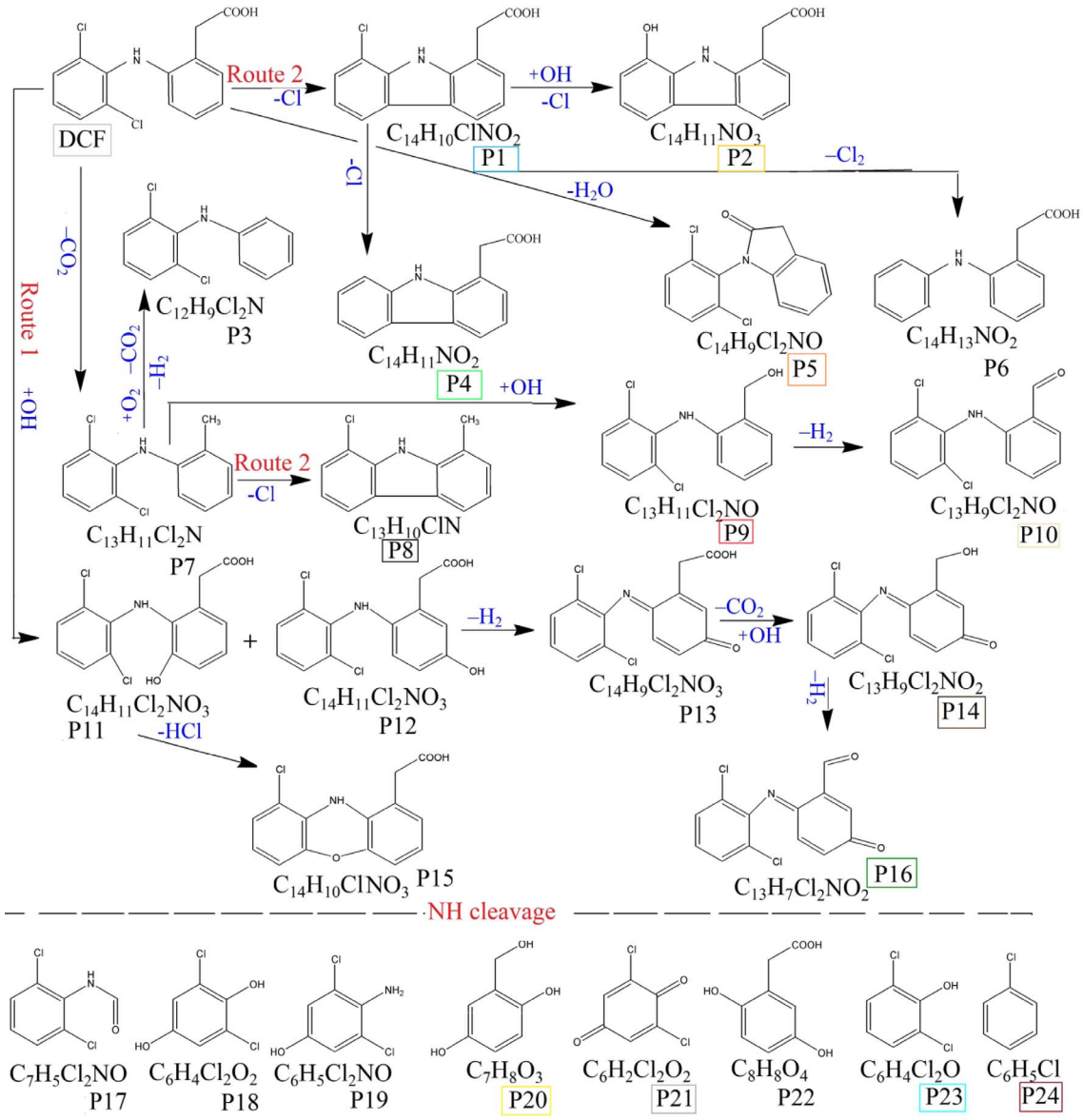

Figure 11. Proposed pathways for the mechanism of DCF photodegradation on ZnCo catalyst under irradiation by simulated UV-light.

higher mineralization degrees than their MMOs correspondents. The DFC photolysis, photodegradation and photo-mineralization pathways were thoroughly elucidated using a combination between UV–Vis spectroscopy, TOC and LC-MS techniques. These results were deeply exploited for the identification of the resulted degradation intermediates. The degradation pathways of DCF could be elucidated by considering the catalyst response as a function of the type of light used for irradiation. The best results, e.g. 96% photodegradation with ~85% mineralization of DFC, were obtained by using only 1 g ZnCo LDH-type photocatalyst per 1 L of DFC aqueous solution and solar light irradiation, thus indicating that a perfor-

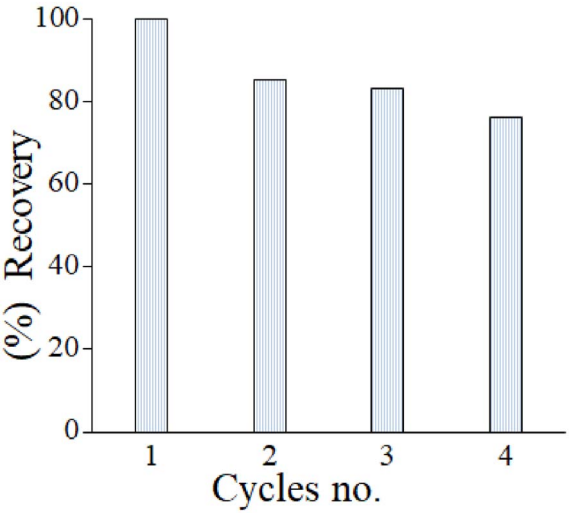

Figure 12. ZnCo catalyst performance recovery for DCF photodegradation under solar light.

mant and economically viable technology for large scale decontamination of polluted aqueous environments can be developed.

Conflicts of interest

Authors have no conflict of interest to declare.

Acknowledgements

EMS acknowledges the fund for scientific research flanders (FWO—Vlaanderen) for financial support. GC is grateful for the financial supports from the grant-in-aid for scientific research from Romanian National Authority for Scientific Research, CNCS-UEFISCDI (PN-II-ID-1751). PC acknowledges the FWO-Flanders (project no. G038215N) for financial support. EFG thanks his colleague R. G. Ciocarlan from the Laboratory of Adsorption and Catalysis of University of Antwerp for technical and analytical assistance in the laboratory. We furthermore thank Professors K. De Wael and G. Nuyts from AXES, University of Antwerp for performing SEM/EDX measurements.

Supplementary data

Supporting information for this article is available on the journal's website under https://doi.org/10.5802/crchim.167 or from the author.

References

[1] B. Di Credico, I. R. Bellobono, M. D'Arienzo, D. Fumagalli, M. Redaelli, R. Scotti, F. Morazzoni, *Int. J. Photoenergy*, 2015, **2015**, 1-13.
[2] P. Sathishkumar, R. Anu, A. Meena, T. Palanisami, *Sci. Total Environ.*, 2020, **698**, 134057-134088.
[3] T. Aus der Beek, F.-A. Weber, A. Bergmann, S. Hickmann, I. A. Ebert, A. K. Hein, *Environ. Toxicol. Chem.*, 2016, **35**, 823-835.
[4] I. C. Guiloski, J. Luiz, C. Ribas, S. Pereira, A. Paula, P. Neves, H. Cristina, S. De Assis, *Environ. Saf.*, 2015, **114**, 204-211.
[5] R. Loos, D. Marinov, I. Sanseverino, D. Napierska, T. Lettieri, "Review of the 1st Watch List Under the Water Framework Directive and Recommendations for the 2nd Watch List", Tech. Report EUR 29173 EN, Publications Office of the European Union, Luxembourg, 2018.
[6] Y. Zhang, S. Geißzen, C. Gal, *Chemosphere*, 2008, **73**, 1151-1161.
[7] P. Bartels, W. von Tümpling Jr., *Sci. Total Environ.*, 2007, **374**, 143-155.
[8] L. Lonappan, S. K. Brar, R. K. Das, M. Verma, R. Y. Surampalli, *Environ. Int.*, 2016, **96**, 127-138.
[9] X. Hu, J. Yang, J. Zhang, *J. Hazard. Mater.*, 2011, **196**, 220-227.
[10] Z. Hu, X. Cai, Z. Wang, S. Li, Z. Wang, X. Xie, *J. Hazard. Mater.*, 2019, **380**, 120812-120826.
[11] E. Mugunthan, M. B. Saidutta, P. E. Jagadeeshbabu, *J. Photochem. Photobiol. A Chem.*, 2019, **383**, 111993-112005.
[12] V. C. Sarasidis, K. V. Plakas, S. I. Patsios, A. J. Karabelas, *Chem. Eng. J.*, 2014, **239**, 299-311.
[13] S. Salaeh, D. Juretic Perisic, M. Biosic, H. Kusic, S. Babic, U. Lavrencic Stangar, D. D. Dionysiou, A. Loncaric Bozic, *Chem. Eng. J.*, 2016, **304**, 289-302.
[14] W. Zhang, L. Zhou, H. Deng, *J. Mol. Catal. A Chem.*, 2016, **423**, 270-276.
[15] M. Darie, E. M. Seftel, M. Mertens, R. G. Ciocarlan, P. Cool, G. Carja, *Appl. Clay Sci.*, 2019, **182**, 105250-105259.
[16] D. Gilea, T. Radu, M. Muresanu, G. Carja, *Appl. Surf. Sci.*, 2018, **444**, 407-413.
[17] F. Cavani, F. Trifirb, A. Vaccari, *Catal. Today*, 1991, **11**, 173-301.
[18] X. Long, Z. Wang, S. Xiao, Y. An, S. Yang, *Mater. Today*, 2016, **19**, 213-226.
[19] L. Wang, X. Gao, J. Su, Q. Zhang, K. Zheng, Z. Zhang, *J. Photochem. Photobiol. A Chem.*, 2019, **383**, 111973-111983.
[20] A. Alvarez-Martin, S. Trashin, M. Cuykx, A. Covaci, *Dye. Pigment.*, 2017, **145**, 376-384.
[21] F. T. L. Muniz, M. A. Ribeiro Miranda, C. Morilla dos Santos, J. M. Sasaki, *Acta Crystallogr. A*, 2016, **72**, 385-390.
[22] E. M. Seftel, E. Popovici, M. Mertens, K. De Witte, G. Van Tendeloo, P. Cool, E. F. Vansant, *Microporous Mesoporous Mater.*, 2008, **113**, 296-304.

[23] J. Prince, F. Tzompantzi, G. Mendoza-Damián, F. Hernández-Beltrán, J. S. Valente, *Appl. Catal. B Environ.*, 2015, **163**, 352-360.
[24] G. Carja, E. F. Grosu, M. Mureseanu, D. Lutic, *Catal. Sci. Technol.*, 2017, **7**, 5402-5412.
[25] A. Ulibarri, J. M. Fernindez, F. M. Labajos, V. Rives, *Chem. Mater.*, 1991, **3**, 626-630.
[26] S. Murgolo, I. S. Moreira, C. Piccirillo, P. M. L. Castro, G. Ventrella, C. Cocozza, G. Mascolo, *Materials (Basel)*, 2018, **11**, 1779-1795.
[27] B. Czech, K. Rubinowska, *Adsorption*, 2013, **19**, 619-630.
[28] P. Chen, Q. Zhang, Y. Su, L. Shen, F. Wang, H. Liu, *Chem. Eng. J.*, 2018, **332**, 737-748.
[29] W. Liu, Y. Li, F. Liu, W. Jiang, D. Zhang, J. Liang, *Water Res.*, 2019, **151**, 8-19.
[30] M. Giahi, *Russ. J. Appl. Chem.*, 2015, **88**, 2044-2049.
[31] E. Mugunthan, M. B. Saidutta, P. E. Jagadeeshbabu, *Environ. Technol.*, 2017, **40**, 929-941.
[32] W. L. da Silva, M. A. Lansarin, J. H. Z. Dos Santos, F. Silveira, *Water Sci. Technol.*, 2016, **74**, 2370-2383.
[33] J. A. Morales-Zarate, S. P. Paredes-Carrera, L. V. Castro-Sotelo, *Rev. Mex. Ing. Química*, 2018, **17**, 941-953.
[34] E. I. Moreno-Valencia, S. P. Paredes-Carrera, J. C. Sánchez-Ochoa, S. O. Flores-Valle, J. R. Avendaño-Gómez, *Mater. Res. Express*, 2017, **4**, 115026-115044.
[35] E. I. Moreno-Valencia, S. P. Paredes-Carrera, J. C. Sánchez-Ochoa, S. O. Flores-Valle, J. R. Avendano-Gómez, *Mater. Res. Express*, 2017, **4**, article no. 115026.
[36] J. Bandara, J. A. Mielczarski, J. Kiwi, *Langmuir*, 1999, **15**, 7680-7687.
[37] T. S. Anirudhan, P. L. Divya, J. Nima, S. Sandeep, *J. Colloid Interface Sci.*, 2014, **434**, 48-58.
[38] S. K. Alharbi, J. Kang, L. D. Nghiem, J. P. van de Merwe, F. D. L. Leusch, W. E. Price, *Process Saf. Environ. Prot.*, 2017, **112**, 222-234.
[39] J. Deng, Y. Shao, N. Gao, C. Tan, S. Zhou, X. Hu, *J. Hazard. Mater.*, 2013, **262**, 836-844.
[40] A. Agüera, L. A. Perez Estrada, I. Ferrer, E. M. Thurman, S. Malato, A. R. Fernandez-Alba, *J. Mass Spectrom.*, 2005, **40**, 908-915.
[41] R. Salgado, V. J. Pereira, G. Carvalho, R. Soeiro, V. Gaffney, C. Almeida, V. V. Cardoso, E. Ferreira, M. J. Benoliel, T. A. Ternes, A. Oehmen, M. A. M. Reis, J. P. Noronha, *J. Hazard. Mater.*, 2013, **244–245**, 516-527.
[42] A. R. Banaschik, H. Jablonowski, J. Patrick, J. F. Kolb, *J. Hazard. Mater.*, 2017, **342**, 651-660.
[43] M. Gavrilescu, K. Demnerova, J. Aamand, S. Agathos, F. Fava, *Biotechnology*, 2015, **32**, 147-156.